Original Research Article

Open Access

Omniscient Pte.Ltd.

Investigation of Elevated Temperature Strengths of Cold-Formed Austenitic Hollow Section Beams with a Web Hole

Andy Prabowo*, Jonathan Chen

Department of Civil Engineering, Universitas Tarumanagara, Jakarta, 11440, Indonesia.

***Correspondence to:**Andy Prabowo, Department of Civil Engineering, Universitas Tarumanagara, Jl. Let. Jend. S. Parman No. 1 West Jakarta, 11440, Indonesia; Email: andy.prabowo@ft.untar.ac.id
Received: April 04, 2025; **Accepted:** April 25, 2025.

Abstract: The steel structure is often used as a building structure because it makes the self-weight lighter than concrete while it has relatively high strength. However, the strength and performance of steel structures will deteriorate when caught in fire due to the rising room temperature. Such deterioration occurs in all types of metallic materials, including stainless steel. Until now, investigation on the performance of stainless steel structures at elevated temperatures is still limited, especially on the strength and performance of Square/Rectangular Hollow Section (SHS/RHS) beams. This study investigates the strength predictions for SHS/RHS beams at elevated temperatures dominated by pure bending failure. An additional web hole located at the mid-span was considered, which further deteriorated the SHS/RHS strengths. The investigation was limited to SHS/RHS beams fabricated from cold-formed austenitic (EN 1.4301) sheets. Data on cross-sectional strengths were obtained from numerical analyses using the finite element programme. Results from the numerical analyses exhibited strength deterioration as the temperature rose. Evaluation of the current strength predictions for the cold-formed SHS/RHS austenitic beams using the Direct Strength Method (DSM) showed conservative but not necessarily safe for the condition at elevated temperatures. The proposed modification led to more conservative and reliable, including for the condition at elevated temperatures.
Keywords: Austenitic stainless steel; Elevated temperatures; Fire resistance design; Web hole

1. Introduction

Stainless steel is known to be superior for its corrosion-resistant properties, while this material can be used to fabricate cold-formed steel sections. Stainless steel contains nickel and chromium, which can prevent further oxidation to stop the formation of rust. Thus, the use of stainless steel becomes relatively more cost-effective compared to carbon steel, as stainless steel does not require painting expenses to reduce rust formation during its service life [1]. This also makes the maintenance costs of stainless steel structures relatively low due to their durability.

The mechanical properties of stainless steel demonstrate its suitability as a material for building construction [2]. These mechanical properties are not limited to tensile strength, elongation, corrosion resistance, weldability,

heat resistance, hardness, compressive strength, impact strength, flexural strength, yield strength, wear resistance, and vibration−damping properties. Compared to carbon steel, stainless steel performs significantly better in terms of fire resistance and maintaining strength and stiffness at extreme temperatures [3].

The mechanical properties of stainless steel differ significantly from those of carbon steel, particularly in terms of strength and ductility. For carbon steel and low−alloy steel, the proportional limit is assumed to be at least 70% of the yield point, but for stainless steel, the proportional limit ranges between 36% and 60% of the yield strength [4]. Therefore, structural design specifications calculated for carbon steel cannot be directly adopted for stainless steel without adjustments, such as in strength calculations for structures at high temperatures.

Stainless steel comes in several types, with one of the most widely used classes being austenitic (EN 1.4301), particularly in household appliances and automotive applications. Austenitic stainless steel contains approximately 0.03% carbon, 18% chromium, and 8% nickel, giving it excellent ductility, weldability, and corrosion resistance [5], making it suitable for use as a structural material.

The testing of stainless steel material properties at high temperatures was conducted by Chen and Young [4]. The test involved two types of stainless steel, duplex (EN 1.4462) and austenitic (EN 1.4301), with a plate thickness of 2 mm. The tests were performed using both the steady−state and transient−state methods with varying temperatures. The yield strength, elastic modulus, and thermal elongation obtained from the tests were compared with predictions found in international specifications [4].

Subsequently, the experimental investigation of the material properties of lean duplex stainless steel (EN 1.4162) at high temperatures was conducted by Huang and Young [6]. The specimens for the tests were taken from the cold−formed hollow steel profiles in square (SHS) and rectangular (RHS) hollow sections. Tensile coupon tests were performed using the steady−state method at different temperatures ranging from 24 to 900°C. Additionally, tensile tests were also conducted using the transient−state method at stress levels ranging from 0 to 750 MPa [6] under predetermined temperature variations.

The research findings from Chen & Young [4] and Huang & Young [6], which proposed empirical models to derive the stress−strain diagrams of stainless steel materials at high temperatures, were adopted in studies Huang et al. [5] and Huang and Young [7] to investigate the design calculations for the strength of beam−column structures fabricated from stainless steel at high temperatures (22−900°C). The specimens used were cold−formed steel with RHS (Rectangular Hollow Section) profiles. However, both studies examined the flexural strength design of RHS beams at normal and high temperatures for different classes of austenitic and lean duplex stainless steels separately.

This study aims to review the strength predictions of RHS beams made from austenitic (EN 1.4301) grade under both ambient temperature and elevated temperatures. Table 1 shows the material properties at various temperatures measured by Chen and Young [4], which consist of Temperature (T), Young's modulus at T (ET), 0.2% proof stress/yield strength ($f_{0.2,T}$), 2% proof stress ($f_{2,T}$), and ultimate strength ($f_{u,T}$). These material properties were used in the finite element (FE) analyses of cold−formed austenitic SHS/RHS beams to obtain the flexural strength of such beams with a web hole located at the mid−span. A total of 200 FE specimens, having variations of cross−section size, web hole diameter, and elevated temperature properties, were generated in the analyses. Subsequently, results from the FE analyses were used to evaluate the existing and proposed strength predictions. Both predictions are based on the Direct Strength Method [8], which has been popular in cold−formed carbon strength predictions. Evaluations of the existing strength predictions other than Direct Strength Method were conducted by Prabowo et al. [9], and it is shown that the strength predictions were in accurate.

Table 1. Material properties of austenitic (EN 1.4301) grade at ambient temperature [4]

T (oC)	E_T (GPa)	$f_{0.2,T}$ (MPa)	$f_{2,T}$ (MPa)	$f_{u,T}$ (MPa)
22	187	398	452	709
320	194	278	330	497
550	168	237	287	459

2. Numerical Modelling

2.1 Material Properties

Modelling material properties in the ABAQUS

program is key to numerical modelling that replicates the behavior of specimens as observed during testing. To date, experimental studies on steel beams at high temperatures are very rare. Existing research, such as that conducted by Huang et al. [5] and Yan and Gernay [10] relies on numerical simulations to obtain data on the behavior of steel structures at elevated temperatures.

In this study, the constitutive relationship of austenitic stainless steel at high temperatures is derived from the stress–strain relationship proposed by Chen and Young [4], as outlined in equations (2.1)–(2.5). The material properties of austenitic stainless steel at high temperatures ($f_{0.2,T}$, $f_{u,T}$, E_T, $\varepsilon_{u,T}$), which were examined at 320°C, 550°C, 660°C, and 870°C, are calculated based on the material properties at room temperature of 22°C ($f_{0.2}$, f_u, E, ε_u) multiplied by the reduction factor k_x from equation (2.6). The symbol "T" denotes the material properties at temperatures above 22°C. as shown in Table 1. The yield stress ($f_{0.2}$) is obtained by performing an offset of 0.2% on the elastic portion of the stress–strain diagram and extending it until it intersects the initial stress–strain curve. The values of the parameters *a, b, c*, and *N* in equation (2.6) are obtained from Table 2.

$$\varepsilon_T = \frac{f_T - f_{0.2,T}}{E_{0.2,T}} + \varepsilon_{u,T}\left(\frac{f_T - f_{0.2,T}}{f_{u,T} - f_{0.2,T}}\right)^{m_T}, for\ f > f_{0.2} \quad (2.1)$$

$$\varepsilon_T = \frac{f_T - f_{0.2,T}}{E_{0.2,T}} + \varepsilon_{u,T}\left(\frac{f_T - f_{0.2,T}}{f_{u,T} - f_{0.2,T}}\right)^{m_T}, for\ f > f_{0.2} \quad (2.2)$$

$$E_{y,T} = \frac{E_T}{1 + 0{,}002 \times n_T \times E_T / f_{0.2,T}} \quad (2.3)$$

$$n_T = 6 + 0{,}2 \times \sqrt{T} \quad (2.4)$$

$$m_T = 2{,}3 - \frac{T}{1000} \quad (2.5)$$

$$k_x = \frac{X_{,T}}{X} = a - \frac{(T-b)^n}{c} \quad (2.6)$$

with $E_{y,T}$ being the elastic modulus at the yield strength at temperature T°C (MPa), f_T representing the stress at temperature T°C (MPa), n_T being the coefficient for the proposed stress–strain equation at temperature T°C, m_T representing the coefficient for the proposed stress–strain equation at temperature T°C, ε_T being the strain at the ultimate stress at temperature T°C (%), and $\varepsilon_{y,T}$ representing the strain at the yield stress at temperature T°C (%).

Table 2. Coefficient values of equation (2.6) [4]

$X_{,T}$	T (°C)	*a*	*b*	*c*	*N*
$E_{,T}$	$22 \leqslant T < 922$	1	22	900	1
$f_{0.2,T}$	$22 \leqslant T < 300$	1	22	45	0,5
	$300 \leqslant T < 850$	0,63	300	$5{,}7 \times 10^5$	2
	$850 \leqslant T < 1000$	0,1	850	600	0,8
$f_{u,T}$	$22 \leqslant T < 450$	0,7	450	$4{,}8 \times 10^{13}$	5
	$450 \leqslant T < 660$	0,7	450	$1{,}92 \times 10^5$	2
$\varepsilon_{u,T}$	$22 \leqslant T < 180$	1	22	247	1
	$180 \leqslant T < 660$	0,36	180	$6{,}1 \times 10^{16}$	6
	$660 \leqslant T \leqslant 960$	0,16	660	2000	1

The approach to the stress–strain relationship model proposed by Chen and Young [4] has been used in studies on the strength of steel beam–columns at high temperatures, as conducted by Huang et al. [5]. The stress and strain values obtained from the calculations using equations (2.1)–(2.6) are converted into true stress (σ_{true}) and logarithmic plastic strain (ε^{pl}_{true}) using equations (2.7) and (2.8).

$$\sigma_{true} = \sigma \times (1 + \varepsilon) \quad (2.7)$$

$$\varepsilon^{pl}_{true} = ln(1 + \varepsilon) - \frac{\sigma_{true}}{E} \quad (2.8)$$

2.2 Geometric Model

In addition to material property, the geometric modelling of the cold–formed RHS beams with a web hole is set on ABAQUS [11], which was validated against Chen et al.[12] study. That numerical model was used to obtain the ultimate strength values from pure bending failure of RHS beams with a hole in the mid–span. The three–dimensional element type used was the S4R shell element, as this element is widely employed in the numerical modelling of cold–formed steel [5,12]. The mesh size of the flat part was 7 mm × 7 mm, with five elements assigned to the rounded corner part. Mesh refinement was applied surrounding the web hole in order to achieve the accuracy of the numerical model.

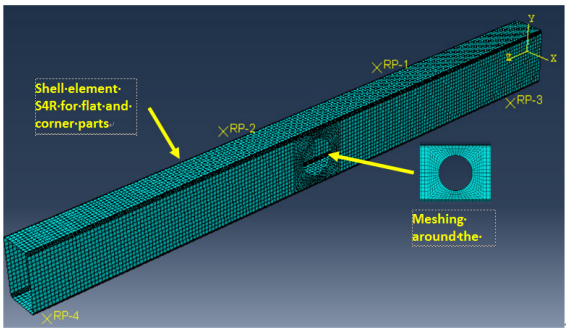

Figure 1. Numerical model of RHS beam under pure bending failure

The RHS structural beam is modelled with two supports beneath the beam's surface. A pinned support is applied on the left side (RP4: displacements in the X, Y, and Z directions are fixed; rotations in the Y and Z directions are fixed), and a roller support is applied on the right side (RP3: displacements in the X and Y directions are fixed; rotations in the Y and Z directions are fixed). The loading is modelled as two concentrated loads (RP1 and RP2: displacement in the X direction is fixed; rotations in the Y and Z directions are fixed) applied on the top surface of the beam (as shown in Figure 1). The static RIKS step is then applied using the displacement control method. The nonlinear geometric parameter (*NLGEOM) is selected to account for the large displacement analysis.

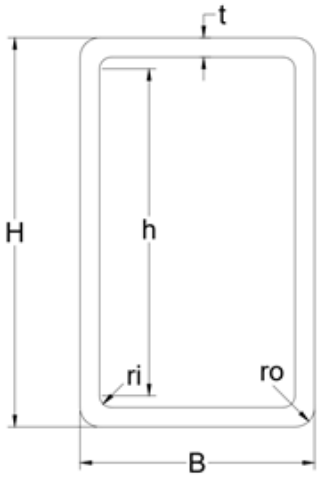

Figure 2. Typical SHS/RHS cross−section

2.3 Validation of Numerical Model

Validation of the numerical model was carried out by comparing the ultimate strength obtained from the experiment [12] and the ABAQUS, as shown in Table 3. The web hole diameter is denoted as the proportion of the flat depth of SHS/RHS cross sections (*D/h*). The typical cross−section drawing can be seen in Figure 2, in which H is overall depth, B is overall width, h is flat depth, ri and ro is the inner and outer radius, respectively.

According to Table 3, it is shown that the ultimate strengths obtained from the numerical model were close to those obtained from the experiment/test, given that the mean of M_{Test}/M_{FEA} was 1.05, with the coefficient of variation (COV) was 1.9%. Moreover, the plot of moment versus rotation curves obtained from the numerical model (FEA) coincided with the test curves, as depicted in Figure 3. Therefore, it was concluded that the numerical model was noteworthy for further parametric study.

Table 3. Ultimate flexural strength ratio (M_{Test}/M_{FEA}) obtained from the experiment (M_{Test}) and ABAQUS (M_{FEA})

Specimen (*H*×*B*×*t*)	*D/h* (%)	M_{Test} (kNm)	M_{FEA} (kNm)	M_{Test}/M_{FEA}
60 × 40 × 4	0	7.59	7.41	1.02
	20	7.54	7.40	1.02
	50	7.12	6.76	1.05
	80	6.23	6.21	1.00
80 × 60 × 4	0	14.49	13.90	1.04
	20	14.43	13.73	1.05
	50	13.67	13.38	1.02
	50 (r)	13.88	13.38	1.04
	80	12.28	11.95	1.03
100 × 40 × 2	0	8.32	7.83	1.06
	20	8.2	7.88	1.04
	50	7.40	7.22	1.02
	50 (r)	7.57	7.22	1.05
	80	6.15	5.83	1.05
120 × 80 × 3	0	21.63	20.16	1.07
	20	21.83	20.14	1.08
	50	20.26	19.05	1.06
	80	17.75	16.04	1.11
			Mean	1.05
			COV	0.019

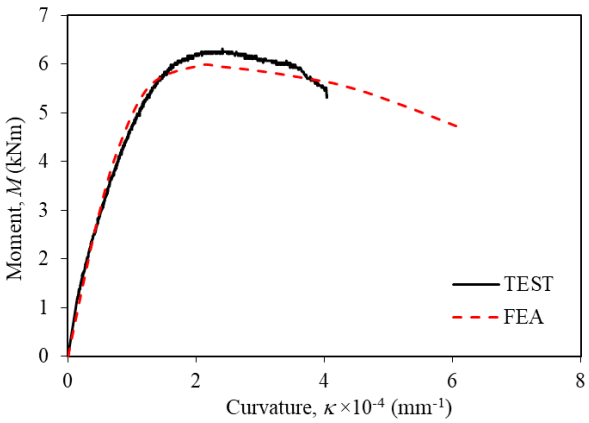

Figure 3. Moment versus curvature curve of specimen 60×40×4D80

The parametric study was conducted to collect the ultimate strength values of cold−formed SHS/RHS beams with a single web hole at the mid−span. In total, 200 numerical specimens were built in ABAQUS, composed of 8 variations of cross−sections (Table 4) and 5 material properties from temperatures mentioned

in Table 1. All cross-sections have 4 variations of *D/h* (20%, 50%, 70%, and 90%), including one extra for sections with *D/h* = 0. All of the parameters were similar to the former studies [12,14] but using different grades of stainless steel. Specimen coding was implemented to distinguish the cross-sectional sizes, proportion of *D/h*, and temperatures. For instance, specimen code 60×40×4D80T320 was given to the cross-section of 60×40×4 having *D/h* of 80% and material properties at 320°C.

The typical failure mode observed in the cross-section of austenitic stainless steel RHS beams when reaching ultimate strength can be seen in Figure 4 and 5. Both figures show the occurrence of local buckling in the top flange of the RHS cross-section, combined with the overall flexural buckling of the entire beam. The local buckling failure takes the form of a sinusoidal wave pattern. At the supports and the two loading points, no deformation occurred due to the activation of constraint nodes before the analysis was run. Shear failure was not observed in any of the numerical analysis results from the ABAQUS. This is evidenced by the absence of local buckling in the region between the supports and the concentrated load locations.

Table 4. Variation of cross-section

H (mm)	*B* (mm)	*t* (mm)	r_i (mm)	r_o (mm)	*H* (mm)
60	40	4	4.4	7.6	60
120	80	3	4.1	6.6	120
300	120	2	4.5	6.5	300
380	286	2	4.5	6.5	380
380	152	1.5	4.7	6.2	380
380	380	4	3.5	7.5	380
380	570	4	3.5	7.5	380
380	570	2	4.5	6.5	380

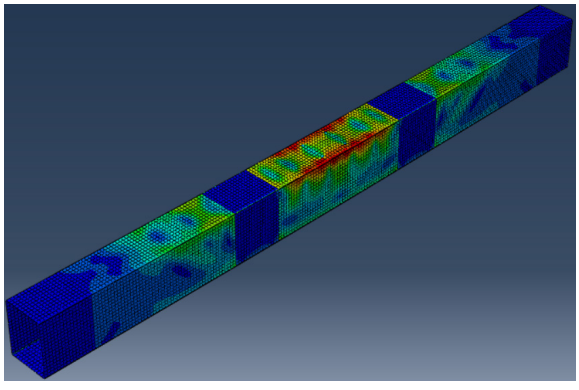

Figure 4. Failure modes of specimen 380× 286× 2D0T22

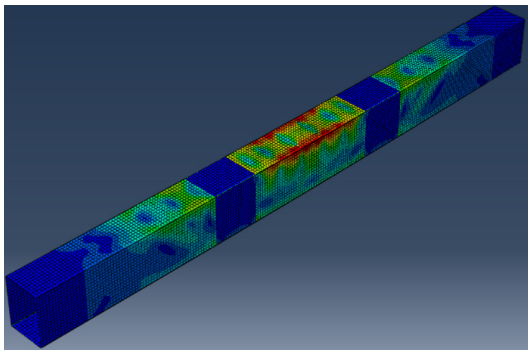

Figure 5. Failure modes of specimen 380× 286 × 2D90T22

3. Flexural Strength Predictions Using Direct Strength Method (DSM) Equations

The Direct Strength Method (DSM) has been used to calculate the strength predictions for cold-formed steel structures under various loading conditions [8]. This method is deemed simpler than the Effective Width Method, which requires iterations and cumbersome calculation steps. However, the DSM equations require elastic buckling load prediction, which can be provided by the CUFSM application developed by [14]. The current design rules for flexural strength prediction specified by ASCE 8 [15] and the proposed strength equations by Chen et al. [12] have utilised the DSM equations. The DSM equations on these two references, including the newest proposal from Priestley and Prabowo [13], will be evaluated in this study for the application of austenitic stainless steel.

3.1 DSM Equations of ASCE 8

The nominal flexural strength of the cross-section according to ASCE 8 (M_{ASCE}) can be determined from the minimum value between the global buckling moment (M_{ne}) and the local buckling moment (M_{nl}), as written in equations (3.1) and (3.2). For RHS sections, the value of M_{ne} will always be determined by yielding failure (M_y), as failure due to torsional buckling will never occur. The value of M_{crl} is obtained using the CUFSM [14], and M_{crl} is expressed as a factor relative to M_y.

$$M_{nl} = M_{ne}\ \lambda_l \leq 0{,}667 \tag{3.1}$$

$$M_{nl} = \left[1 - 0{,}2\left(\frac{M_{crl}}{M_{ne}}\right)^{0{,}4}\right] \times \left(\frac{M_{crl}}{M_{ne}}\right)^{0{,}4} \times M_{ne},\ \lambda_l > 0{,}667 \tag{3.2}$$

Where λ_l is the slenderness factor defined by $(M_{ne}/M_{crl})^{0,5}$) and M_{crl} is the elastic local buckling moment (kNm).

3.2 DSM Equations of Chen et al. [12]

The flexural strength equation using the DSM principle from Chen et al. [12] is aligned with ASCE 8 [15]. The DSM moment ($M^{\#}_{DSM}$) can be determined from the value of M_{nl}. The research by Chen et al. [12] proposed an improvement to the M_{nl} formula based on their findings using ferritic stainless steel. The proposed equations are as follows:

$$M_{nl} = \left[1{,}5 - \frac{0{,}5}{0{,}776} \times \lambda_l\right] \times M_{ne}, \quad \text{for } \lambda_l \le 0{,}776 \tag{3.3}$$

$$M_{nl} = \left[1 - 0{,}15\left(\frac{M_{crl}}{M_{ne}}\right)^{0{,}4}\right] \times \left(\frac{M_{crl}}{M_{ne}}\right)^{0{,}4} \times M_{ne}, \text{ for } \lambda_l > 0{,}776 \tag{3.4}$$

3.3 DSM Equations of Priestley and Prabowo [13]]

The DSM equations (M_{prop}) proposed by Priestley and Prabowo [13] have been formed based on the modified equations proposed by Chen et al. [12], where it is recognised that the strength values of stocky sections ($\lambda_l \le$ a limit value) should be higher than M_y. The DSM equations proposed by Priestley and Prabowo [13] are written in equations (3.5) and (3.6). These equations were developed for lean duplex stainless steel, which aimed to be extended for austenitic stainless steel as well.

$$M_{nl} = \left(1{,}4 - 1\lambda_l\right) \times M_{ne}, \lambda_l \le 0{,}667 \tag{3.5}$$

$$M_{nl} = \left[0{,}8 - 0{,}2\left(\frac{M_{crl}}{M_{ne}}\right)^{0{,}4}\right] \times \left(\frac{M_{crl}}{M_{ne}}\right)^{0{,}4} \times M_{ne}, \quad \lambda_l > 0{,}667 \tag{3.6}$$

4. Reliability Analysis

Reliability analysis is conducted to evaluate the DSM equations of the cold-formed austenitic SHS/RHS beams with a web hole under various temperature conditions. The goal of this reliability analysis is to obtain the reliability index (β_o) for the equations under evaluation. The β_o value must exceed the target value of 2.5 in order to conclude that a set of equations being considered are safe. The β_o value is calculated based on the provisions in ASCE 8 [15], with the equation written as follows:

$$\beta_o = \frac{ln\dfrac{C_\phi \times \ M_m \times F_m \times P_m}{\phi}}{\sqrt{V_M^2 + V_F^2 + C_P V_P^2 + V_Q^2}} \tag{4.1}$$

Where $C\phi$ is the calibration coefficient with a value of 1.52, M_m is the mean value of the material factor (1.25), F_m is the mean value of the fabrication factor (1.0), P_m is the mean value of the ratio between ultimate capacity and nominal capacity, ϕ is the strength reduction factor (0.9), V_m is the coefficient of variation for the material factor (0.1), V_F is the coefficient of variation for the fabrication factor (0.05), V_P is the coefficient of variation for the ratio of ultimate capacity to nominal capacity, V_Q is the coefficient of variation for the load effect (0.21), C_P is the correction factor ($(1+1/n)m/(m-2)$), n is the number of data points, m is the degrees of freedom ($n-1$).

Additionally, the evaluation criteria for assessing the reliability of the DSM equations were performed following Kruppa's recommendations [16]. This method is applied to structures exposed to high temperatures, such as during fires. The focus is on ensuring that the strength obtained from FEA or testing is higher than the predicted design strength. The capacity equation is considered safe if:

- The mean ratio of numerical results to predicted results is on the safe side (mean FEA strength/ DSM strength $\geqslant$ 1).
- The percentage of unsafe results (FEA strength/ DSM strength < 1) is lower than 20%.
- The minimum value of the ratio of FEA strength to DSM predicted strength is at least 0.85.

5. Evaluation of DSM Strength Predictions

All values of M_u were compared to the nominal bending capacity values obtained from equations (3.1)–(3.6). Table 5 shows that the lowest mean values are produced by the equations $M^{\#}_{DSM}$ and M_{prop}. The M_{prop} equation yields the safest and most reliable strength prediction because it has the highest mean value, the reliability index β_o far above 2.5, and the lowest COV. The results of the M_{prop} equation meet the safety criteria of the Kruppa method [16], as all three criteria are fulfilled. In contrast, the DSM equations proposed by ASCE 8 [15] and Chen et al. [12] only meet the reliability criteria set by ASCE 8, although the average ratio between ABAQUS results and DSM equation results is greater than 1. Thus, it can be concluded that while existing DSM equations provide relatively conservative strength predictions, the design rules are not statistically safe (reliable).

Table 5. Evaluations of the strength predictions for cold−formed austenitic SHS/RHS beams with a single web hole

	$\frac{M_u}{M_{ASCE}}$			$\frac{M_u}{M^{\#}_{DSM}}$			$\frac{M_u}{M_{prop}}$		
	D0	D20−D90	D0−D90	D0	D20−D90	D0−D90	D0	D20−D90	D0−D90
Number of Data	40	160	200	40	160	200	40	160	200
Mean	1,24	1,12	1,14	1,11	0,99	1,01	1,44	1,28	1,32
COV	0,249	0,252	0,254	0,146	0,150	0,157	0,117	0,127	0,134
ϕ	0,9	0,9	0,9	0,9	0,9	0,9	0,95	0,95	0,95
β_o	2,73	2,46	2,51	3,03	2,61	2,66	3,97	3,49	3,54
% ratio < 1	15%	41,9%	36,5%	30%	59,4%	53,5%	0%	5%	4%
Smallest ratio	0,93	0,73	0,73	0,9	0,7	0,7	1,02	0,86	0,86

In addition to the evaluation results presented in Table 5, Figure 6 presents the plot of the ratio $\frac{M_u}{M_{ne}}$ for RHS beams, where M_{ne} is calculated using the three DSM equations. The figure shows that the DSM curve from the proposed M_{prop} equation lies below the entire plot of $\frac{M_u}{M_{ne}}$. This is a consequence of the relatively higher mean value compared to the other DSM equations. Additionally, the safety requirement set by the Kruppa method, with a strength ratio > 0.85, makes it challenging to obtain a mean value close to 1.

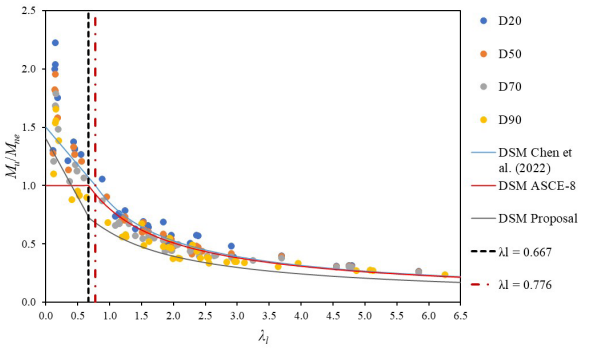

Figure 6. Normalised FEA strengths with M_{ne} plotted with 3 DSM curves

6. Conclusions and Recommendation

The flexural strength equations from the DSM method applied to the cold−formed austenitic SHS/RHS beams with a web hole, according to American specification for cold−formed stainless steel design and the other accompanying studies, provide conservative and statistically safe strength predictions. However, these equations do not meet the safety requirements for structures under elevated temperature condition. The bending strength equation from the proposed DSM method satisfies the safety criteria required by both American specification and criteria for structures at elevated temperatures. Therefore, the proposed equation can be recommended for calculating the pure bending strength of RHS beams with holes at mid−span under high−temperature conditions, such as during a fire. The evaluation of all DSM equations involved in this study uses ABAQUS results from 200 numerical specimens with hole variations ranging from 20−90% of the average web height and simulation temperatures ranging from 20−900°C.

Acknowledgements

The authors would like to thank the Directorate of Research and Community Services Universitas Tarumanagara for providing research grant. The first author is grateful to the second author's contributions as part of his final year project.

Author's Contributions

Andy Prabowo: Conceptual, Methodology, Manuscript Editing, Supervision; Jonathan Chen: Parametric Study, Data Analysis, Manuscript Drafting.

Conflict of Interest

Declaration of conflict of interest.

References

[1] Backhouse A and Baddoo N. Recent developments of stainless steels in structural applications. *Ce/papers*, 2021; 4(2−4):2349−2355. https://doi.org/10.1002/cepa.1560.

[2] Gardner L. Aesthetics, economics and design of stainless steel structures. *Advanced Steel Construction*, 2008; 4(2): 113−122.

[3] Rossi B. Discussion on the use of stainless steel in constructions in view of sustainability. *Thin−*

Walled Structures, 2014; 83:182–189. https://doi.org/10.1016/j.tws.2014.01.021.

[4] Chen J and Young B. Stress–strain curves for stainless steel at elevated temperatures. *Engineering Structures*, 2006; 28(2): 229–239. https://doi.org/10.1016/j.engstruct.2005.07.005.

[5] Huang Y, Chen J, He Y, and Young B. Design of cold–formed stainless steel RHS and SHS beam–columns at elevated temperatures. *Thin–Walled Structures*, 2021; 165: 107960. https://doi.org/10.1016/j.tws.2021.107960.

[6] Huang Y and Young B. Stress–strain relationship of cold–formed lean duplex stainless steel at elevated temperatures. *Journal of Constructional Steel Research*, 2014; 92: 103–113. https://doi.org/10.1016/j.jcsr.2013.09.007.

[7] Huang Y and Young B. Experimental and numerical investigation of cold–formed lean duplex stainless steel flexural members. *Thin–Walled Structures*, 2013; 73:216–228. https://doi.org/10.1016/j.tws.2013.07.019.

[8] Schafer BW. Advances in the Direct Strength Method of cold–formed steel design. Thin–Walled Structures, 2019; 140:533–541. https://doi.org/10.1016/j.tws.2019.03.001.

[9] Prabowo A, Huang Y, Young B. Cold–formed stainless steel beams with single web hole at elevated temperatures. *Thin–Walled Structures,* 2024; 195:111321. https://doi.org/10.1016/j.tws.2023.111321.

[10] Yan X and Gernay T. Local buckling of cold–formed high–strength steel hollow section columns at elevated temperatures. *Journal of Constructional Steel Research*, 2022; 196:107403. https://doi.org/10.1016/j.jcsr.2022.107403.

[11] ABAQUS. *User's manual and theory manual.* Dassault Systèmes Simulia Corp; 2023.

[12] Chen Z, Huang Y, Young B. Design of cold–formed ferritic stainless steel RHS perforated beams. *Engineering Structures*, 2022; 250, 113372. https://doi.org/10.1016/j.engstruct.2021.113372.

[13] Priestley KA and Prabowo, A. Flexural strength of RHS perforated lean duplex stainless steel beam at temperature 24–900ºC. *Civil Engineering Dimension*, 2024; 26(1), 71–80. https://doi.org/10.9744/ced.26.1.71–80.

[14] Adany, S., & Schafer, B. W. Buckling Analysis of Cold–formed Steel Members Using CUFSM. *Paper for Eighteenth International Specialty Conference on Cold–Formed Steel Structures*, 39–54. Orlando, 2006 October 26. Florida. Available from https://scholarsmine.mst.edu/isccss/18iccfss/18iccfss–session1/2.

[15] ASCE–8. *Specification for the design of cold–formed stainless steel structural members. SEI/ASCE8–22*. Reston, Virginia: American Society of Civil Engineers; 2023.

[16] Kruppa J. Eurocodes fire parts: proposal for a methodology to check the accuracy of assessment methods. *CEN TC 250* (*Horizontal Group Fire Document*), 1999. p. 99–130.